TOPOLOGICAL MATTER

Observation of the topological Anderson insulator in disordered atomic wires

Eric J. Meier[1], Fangzhao Alex An[1], Alexandre Dauphin[2], Maria Maffei[2,3], Pietro Massignan[2,4]*, Taylor L. Hughes[1]*, Bryce Gadway[1]*

Topology and disorder have a rich combined influence on quantum transport. To probe their interplay, we synthesized one-dimensional chiral symmetric wires with controllable disorder via spectroscopic Hamiltonian engineering, based on the laser-driven coupling of discrete momentum states of ultracold atoms. Measuring the bulk evolution of a topological indicator after a sudden quench, we observed the topological Anderson insulator phase, in which added disorder drives the band structure of a wire from topologically trivial to nontrivial. In addition, we observed the robustness of topologically nontrivial wires to weak disorder and measured the transition to a trivial phase in the presence of strong disorder. Atomic interactions in this quantum simulation platform may enable realizations of strongly interacting topological fluids.

Topology and disorder share many surprising connections, from the formal similarity of one-dimensional (1D) pseudodisordered lattices and 2D integer quantum Hall Hofstadter lattices (*1*, *2*) to the deep connection between the symmetry classes of random matrices (*3*) and the classification of symmetry-protected topological phases (*4*). Recently, there has been great interest in exploring both disorder (*5*) and topology (*6*) through quantum simulation, stemming from the dramatic influences that these ingredients can have, separately, on the localization properties of quantum particles (*7*, *8*). When combined, disorder and topology can have a rich and varied influence on quantum transport (*9*). Indeed, one of the hallmark features of topological insulators (TIs) is the topologically protected boundary states that are immune to certain types of disorder up to some characteristic strength (*10*). The robust conductance of such boundary states, such as the 1D edge states of integer quantum Hall systems (*8*) or the 2D surface states of 3D TIs (*11*), serves as an important counterexample to the inevitability of localization in low-dimensional disordered systems (*7*, *12*). However, topological features can eventually disappear when the disorder strength becomes too large, and unusual critical phenomena related to the unwinding of the topology can accompany such transitions (*13*, *14*).

Conversely, static disorder can induce nontrivial topology when added to a trivial band structure. This disorder-driven topological phase, known as the topological Anderson insulator (TAI), was first predicted to occur in metallic 2D HgTe/CdTe quantum wells (*15*). There has been much interest in the TAI phase over the past decade (*15*–*17*), and many theoretical studies have shown the TAI phenomenon to be quite general, emerging across a range of disordered systems (*18*–*21*). However, owing to the lack of precise control over disorder in real materials and the difficulty in engineering both topology and disorder in most quantum simulators, the TAI has so far evaded experimental realization. In this work, we reach this goal by engineering synthetic 1D chiral symmetric wires with precisely controllable disorder using simultaneous, coherent control over many transitions between discrete quantum states of ultracold atoms.

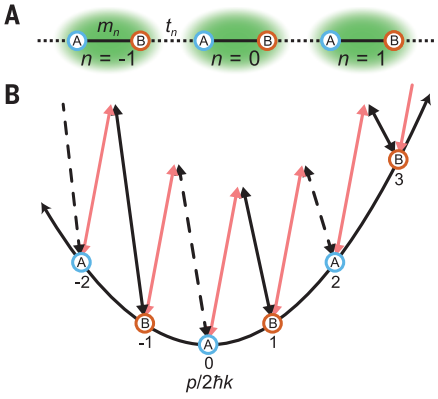

Fig. 1. Synthetic chiral symmetric wires engineered with atomic momentum states. (**A**) Schematic lattice of the nearest-neighbor-coupled chiral symmetric wire. Site-to-site links within the unit cell (solid) and those connecting different unit cells (dashed) have independent tunneling energies m_n and t_n, respectively. (**B**) Schematic of the experimental implementation of the tight-binding model depicted in (A), with tunnelings based on two-photon Bragg transitions between discrete atomic motional states with momentum p.

The topological band structures we consider are 1D TIs based on the Su-Schrieffer-Heeger model with a chiral, or sublattice, symmetry (*4*, *19*, *22*, *23*). We describe this system in terms of a tight-binding model with a two-site unit cell, consisting of sublattice sites A and B (depicted in Fig. 1A). We consider the Hamiltonian

$$H = \sum_n \left[m_n c_n^\dagger S c_n + t_n \left(c_{n+1}^\dagger \frac{(\sigma_1 - i\sigma_2)}{2} c_n + \text{h.c.} \right) \right] \quad (1)$$

where $c_n^\dagger = (c_{n,\text{A}}^\dagger, c_{n,\text{B}}^\dagger)$ creates a particle at unit cell n in sublattice site A or B, c_n is the corresponding annihilation operator, h.c. denotes the Hermitian conjugate, and σ_i are the Pauli matrices related to the sublattice degree of freedom (*23*). The m_n and t_n characterize the intra- and intercell tunneling energies, respectively. This model can describe chiral wires of the AIII or BDI symmetry classes, by choosing the intracell hopping term to be $S = \sigma_1$ (BDI) or $S = \sigma_2$ (AIII). Both the AIII (chiral unitary) and the BDI (chiral orthogonal) class models respect chiral symmetry—that is, they obey $\Gamma H \Gamma = -H$ with the chiral operator $\Gamma = \sigma_3 \otimes \mathbb{I}$—whereas the BDI class also obeys particle-hole and time-reversal symmetries (*4*). In this work we chose to study both BDI and AIII class systems because they represent all possible distinguishable chiral classes for which the $\mathbb{Z}$ topological invariant in one dimension, the winding number, is defined.

We experimentally implement effective tight-binding models of the form of Eq. 1 using the controlled, parametric coupling of many discrete momentum states of ultracold atoms (*24*). We start with a weakly trapped Bose-Einstein condensate (BEC) of ^{87}Rb atoms and apply a pair of counter-propagating laser fields with nominal wavelength λ and wave vector $k = 2\pi/\lambda$. These lasers are far-detuned from any atomic transition; however, their interference pattern couples to the atoms through the ac Stark effect. The spatial periodicity of the laser interference pattern, π/k, defines the set of momentum states whose momenta are separated by integer values of $2\hbar k$ (where $\hbar = 2\pi\hbar$ is the Planck constant). Atoms initially in the BEC, which is a source of atoms with essentially zero momentum, may undergo transitions between these many discrete momentum states, which represent the sites of our synthetic lattice. The effective tunneling of atoms between these sites is precisely controlled by simultaneously driving many two-photon Bragg transitions with the applied laser fields. The individual, spectroscopically resolved control over many such transitions is allowed for by the Doppler shifts experienced by the atoms, which are specific to the various Bragg transitions

[1]Department of Physics, University of Illinois at Urbana–Champaign, Urbana, IL 61801-3080, USA. [2]ICFO–Institut de Ciencies Fotoniques, The Barcelona Institute of Science and Technology, 08860 Castelldefels, Barcelona, Spain. [3]Dipartimento di Fisica, Università di Napoli Federico II, Complesso Universitario di Monte Sant'Angelo, Via Cintia, 80126 Napoli, Italy. [4]Departament de Física, Universitat Politècnica de Catalunya, Campus Nord B4-B5, 08034 Barcelona, Spain.
***Corresponding author. Email: bgadway@illinois.edu (B.G.); hughest@illinois.edu (T.L.H.); pietro.massignan@upc.edu (P.M.)**

Downloaded from http://science.sciencemag.org/ on December 23, 2018

(Fig. 1B). This provides local (in momentum space) control of the intra- and intercell tunneling amplitudes and phases, directly through the amplitudes and phases of the corresponding Bragg laser fields (*24*). This control gives us access to both BDI and AIII class wires, in contrast to previous studies based on real-space superlattices that were restricted to exploring BDI wires, because quantum tunneling between stationary lattice sites is real-valued (*25*–*27*).

The ability to create precisely defined disorder in the off-diagonal tunneling terms is crucial for this study. Unlike the site-potential disorder that is more naturally realized in real-space cold atom experiments—for example, through optical speckle (*28*) or quasiperiodic lattice potentials (*29*)—pure tunneling disorder is important for preserving the chiral symmetry of our wires (*19*, *23*). In particular, we let

$$t_n = t(1 + W_1\omega_n) \tag{2}$$

$$m_n = t(m + W_2\omega'_n) \tag{3}$$

define the controlled fluctuations of our hopping terms, where t is the characteristic intercell tunneling energy, m is the ratio of intra- to intercell tunneling in the clean limit, ω_n and ω'_n are independent random real numbers chosen uniformly from the range [−0.5, 0.5], and W_1 and W_2 are the dimensionless disorder strengths applied to inter- and intracell tunneling.

We begin by considering the influence of disorder added to a BDI-class wire. The wire is strongly dimerized, as characterized by a small intracell-to-intercell tunneling ratio of $m = 0.100(5)$ (with $t/\hbar \approx 2\pi \times 1.2$ kHz), and hence is in the topological regime in the clean limit. We fix the disorder amplitudes to be $W \equiv W_2 = 2W_1$ and show in Fig. 2A the disorder-averaged topological phase diagram of this model as a function of W and m, as determined numerically by a real-space calculation of the winding number ν for a system with 200 unit cells, together with the critical phase boundary predicted for an infinite system based on the divergence of the localization length Λ (*23*, *30*).

The strong dimerization produces a large (in units of the bandwidth) energy gap in the band structure. Such large bandgaps are typically favorable for experimentally observing the topological nature of disorder-free nontrivial wires via adiabatic charge pumping (*25*, *26*) or the adiabatic preparation of boundary states (*31*). However, it is expected that in disordered chiral symmetric wires, the bulk energy gap will essentially vanish at moderate disorder strengths, well below those required to induce a change in topology (*23*). The energy gap is replaced by a mobility gap, and the band insulator of the clean system is replaced by an Anderson insulator that remains topological, with topology carried by localized states in the spectrum (*23*). Thus, without the spectral gap, experimental probes relying on adiabaticity are expected to fail in evidencing the topology of disordered wires.

We instead characterize the topology of our wires by monitoring the bulk dynamical response of atoms to a sudden quench. Specifically, we measure the mean chiral displacement of our atoms. This observable was recently introduced in the context of discrete-time photonic quantum walks (*32*); here we measure it for continuous-time dynamics. We define the expectation value of the chiral displacement operator as

$$\mathcal{C} = 2\langle \Gamma X \rangle \tag{4}$$

given in terms of the chiral operator Γ and the unit cell operator X (*32*). The dynamics of $\mathcal{C}$, in general, display a transient, oscillatory behavior, and their time- and disorder-average $\langle \bar{\mathcal{C}} \rangle$ converges to the winding number ν, or equivalently to the Zak phase φ_{Zak} divided by π, in both the clean and the disordered cases. Moreover, at topological critical points, $\langle \bar{\mathcal{C}} \rangle$ converges to the average of the invariants computed in the two neighboring phases (*30*, *32*, *33*).

For our experiment, we begin with all tunnel couplings turned off, and the entire atomic population localized at a single central bulk lattice site (site A of unit cell $n = 0$, for a system with 20 unit cells). We then quench on the tunnel couplings in a stepwise fashion. The projection of the localized initial state onto the quenched system's eigenstates leads to rich dynamics, as depicted in Fig. 2B for both weak ($W = 0.5$) and strong ($W = 5$) disorder. Such site-resolved dynamics of the atomic population distribution are directly measured by a series of absorption images taken after dynamical evolution under the Hamiltonian of Eq. 1 for a variable time τ (given in units

Downloaded from http://science.sciencemag.org/ on December 23, 2018

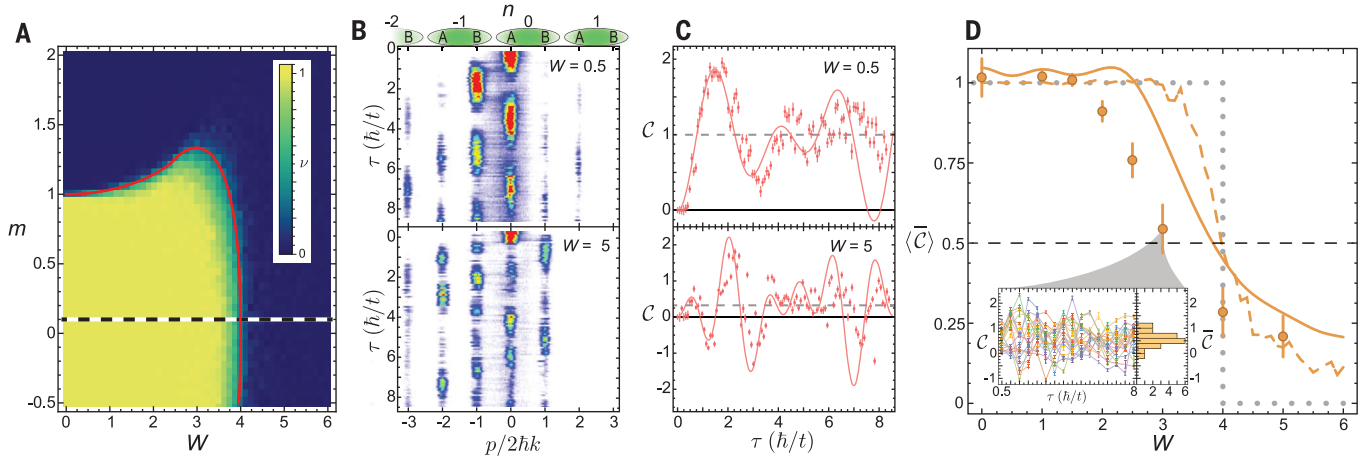

Fig. 2. Disorder-driven transition from topological to trivial wires. (**A**) Calculated topological phase diagram of the BDI wire model described in Eq. 1, showing the winding number ν (inset color scale) as a function of disorder strength W and tunneling ratio m with tunneling disorder strengths $W \equiv W_2 = 2W_1$. The striped black and white line at $m = 0.1$ indicates the region explored experimentally in (B) to (D). The solid red curve indicates the critical phase boundary (i.e., the set of points where the localization length Λ diverges for an infinite chain) (*23*, *30*). (**B**) Integrated absorption images of the bulk dynamics after a sudden quench of the tunnel couplings, for both weak disorder ($W = 0.5$) and strong disorder ($W = 5$), each for a single disorder configuration. (**C**) Dynamics of $\mathcal{C}$ calculated from the data shown in (B). The solid red curves are numerical simulations according to Eq. 1 with no free parameters (*30*). The dashed gray horizontal lines denote $\bar{\mathcal{C}}$ for each dataset. (**D**) $\langle \bar{\mathcal{C}} \rangle$ as a function of W for $m = 0.100(5)$. The data are averaged over 20 independent disorder configurations and times in the range 0.5 $\hbar/t$ to 8 $\hbar/t$ in steps of 0.5 $\hbar/t$. The solid gold line represents a numerical simulation according to Eq. 1, with no free parameters for 200 disorder configurations but with the same finite-time sampling as the data (*30*). The dashed gold line is based on the same simulation as the solid gold line but sampled to much longer times (τ = 1000 $\hbar/t$) in a wire with 250 unit cells (*30*). The dotted gray curve shows the topological index in the thermodynamic limit (*23*), which changes value at the same point as the red line position in (A). This topological index takes a value of 0.5 at the critical point, as indicated by the horizontal dashed line. The inset shows $\mathcal{C}$ for $W = 3$ as a function of time for all 20 disorder configurations (distinguished by color) with the number of disorder configurations corresponding to various values of $\bar{\mathcal{C}}$ shown in the histogram. All error bars in (C) and (D) denote one standard error of the mean.

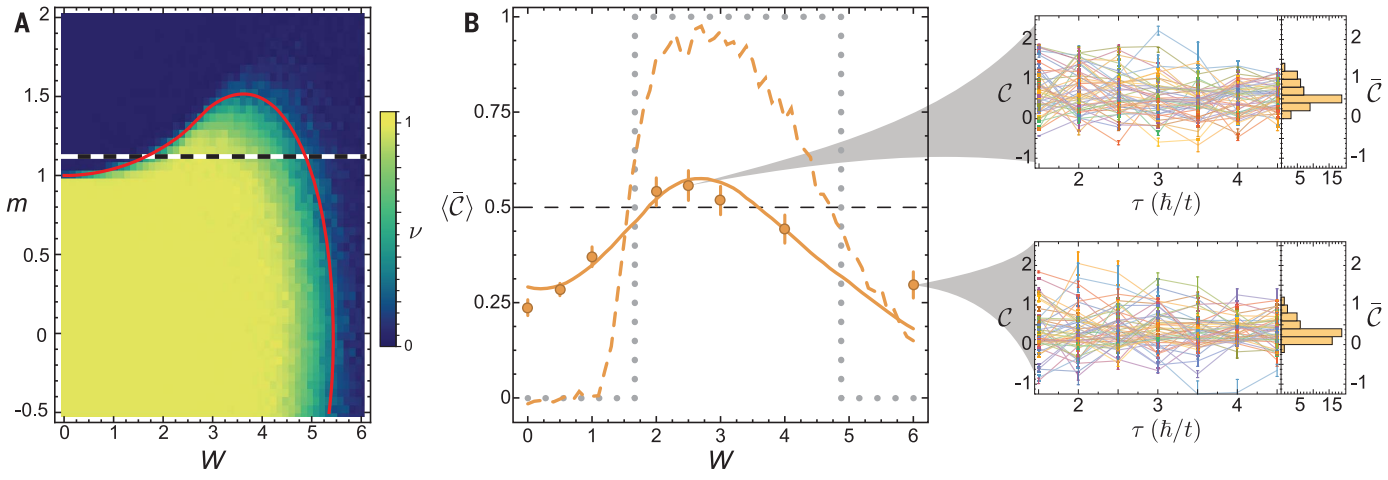

Fig. 3. Observation of the TAI phase. (**A**) Calculated topological phase diagram of the AIII wire model described in Eq. 1, showing the computed winding number (color scale at right) as a function of disorder strength W and tunneling ratio m with tunneling disorder strengths $W \equiv W_2$ ($W_1 = 0$). The striped black and white line at $m = 1.12$ indicates the region explored experimentally in (B). The solid red curve indicates the critical boundary (i.e., the set of points where the localization length Λ diverges for an infinite chain) (*23*, *30*). (**B**) $\langle \bar{C} \rangle$ as a function of W for $m = 1.12(2)$. The data are averaged over 50 independent disorder configurations and are averaged in time over the range 1.5 $\hbar/t$ to 4.5 $\hbar/t$ in steps of 0.5 $\hbar/t$. The solid gold line shows a numerical simulation according to Eq. 1 for 200 disorder configurations but with the same finite-time sampling as the data (*30*). The dashed gold line is based on the same simulation as the solid gold line but sampled to much longer times ($\tau = 1000\ \hbar/t$) in a 250–unit cell system (*30*). The dotted gray curve shows the topological index in the thermodynamic limit (*23*), which changes value at the same point as the red line position in (A). This topological index takes a value of 0.5 at the critical points, as indicated by the horizontal dashed line. $\mathcal{C}$ as a function of time for all 50 disorder realizations (distinguished by color) is shown at the right for $W = 2.5$ and 6; histograms of $\bar{\mathcal{C}}$ are shown to the right of each plot. All error bars in (B) denote one standard error of the mean.

of the tunneling time $\hbar/t \approx 130\ \mu s$) and after the discrete momentum states separate according to their momenta during a time-of-flight period (*24*). From the data shown in Fig. 2B, we calculate $\mathcal{C}$ as a function of τ as shown in Fig. 2C, along with the time average $\bar{\mathcal{C}}$. We additionally obtain the disorder-averaged topological characterization of the system $\langle \bar{\mathcal{C}} \rangle$ by averaging $\bar{\mathcal{C}}$ over many independent disorder configurations.

The dependence of $\langle \bar{\mathcal{C}} \rangle$ on the strength of applied disorder W is summarized in Fig. 2D. The inset of Fig. 2D depicts the determination of $\langle \bar{\mathcal{C}} \rangle$ (shown for the case $W = 3$), first from the time average of $\mathcal{C}$ over 16 values of τ evenly spaced between $0.5\hbar/t$ and $8\hbar/t$, followed by an average over 20 unique realizations of disorder. We observe that $\langle \bar{\mathcal{C}} \rangle$ is robust to weak disorder, maintaining a nearly quantized value close to 1. For strong disorder, $W \gtrsim 2$, we observe a relatively steep drop in $\langle \bar{\mathcal{C}} \rangle$, with it falling below $\langle \bar{\mathcal{C}} \rangle = 0.5$ for $W \gtrsim 3$. Our observed decrease of $\langle \bar{\mathcal{C}} \rangle$ with increasing disorder is in reasonably good agreement with a numerical simulation (solid gold line in Fig. 2D) of the Hamiltonian in Eq. 1 for experimental time scales. The observed decay of $\langle \bar{\mathcal{C}} \rangle$ is associated with a disorder-driven transition between topological ($W \lesssim 4$) and trivial wires ($W \gtrsim 4$).

On an infinitely long chain, we would expect to observe a sharp phase transition in the infinite-time limit of our $\langle \bar{\mathcal{C}} \rangle$ measurement, yielding quantized values of the invariant for all disorders, and half-integer values at the critical phase boundary (*30*, *34*). However, we instead observe a smooth crossover owing to broadening from our finite period of quench dynamics and the corresponding finite number of sites. The observation of a moderately sharper transition, such as that of the dashed-line numerical simulation in Fig. 2D, would require that we measure at extremely long time scales (shown for 1000 tunneling times) and for very large systems (shown for 250 unit cells), which at the moment is beyond the capabilities of our experimental technique (*30*). The slow convergence of this transition with increasing measurement time and system size is a characteristic feature of random-singlet transitions (*14*), such as those found in chiral symmetric wires at strong disorder.

Having demonstrated a disorder-driven change of topology in BDI-class wires, we now turn our attention to AIII-class wires, for which we investigate the surprising feature that an initially clean, trivial system can be driven topological through the addition of disorder. This phenomenon is manifest in the calculated phase diagram of AIII-class wires shown in Fig. 3A for m just exceeding 1. The value $|m| = 1$ is the critical point between the topological and trivial phase in the clean limit, and values of $|m| > 1$ are in the trivial phase in the absence of disorder. However, we see that random tunneling disorder induces the TAI phase over a broad range of weak to moderate W values, eventually giving way to a trivial Anderson insulator phase again for very large disorder. Beyond numerics, a mechanism for the formation of a TAI phase was first elaborated in (*17*) for 2D systems. In that work, disorder is taken into account perturbatively using the self-consistent Born approximation and was shown to effectively renormalize the parameters in the Hamiltonian [including the parameter(s) that tune between the topological and trivial phases]. The TAI phase arises because, as disorder is added to the trivial phase tuned near the clean critical point, the effective Hamiltonian is renormalized through the critical point and into the topological phase. This type of reasoning was adapted, with strong support from numerical evidence, and extended to describe the TAI phase in 1D systems, including both the BDI- and AIII-class wires that we consider here (*19*, *23*, *34*).

Here we probe the influence of tunneling disorder on atomic wires of the AIII class. Because we are interested in the TAI phase, we start with a slight dimerization [$m = 1.12(2)$] that places the system in a trivial phase in the clean limit. We note that being so near the critical point at $m = 1$ causes the bandgap in the clean limit to be much smaller than in the previous experimental setup. The choice of disorder we consider here differs from the previous case: We add disorder only to the intracell hopping terms, that is, setting $W_1 = 0$ and $W \equiv W_2$. The difference in the topological phase diagrams for the BDI case (Fig. 2A) and the AIII case (Fig. 3A) comes entirely from this change in disorder configuration. In one dimension, the topological phase diagrams for BDI and AIII systems are identical when exposed to equivalent disorder configurations (W_1 and W_2 values) and with only nearest-neighbor tunnelings present. From (*17*, *19*, *34*), we expect that, for weak disorder of this form, the intracell hopping m should be renormalized toward the topological phase, resulting in a TAI. Thanks to the smaller bandgap in this case of reduced dimerization, the effects of off-resonant driving (*24*, *30*) in our system become more pronounced. To mitigate these effects, we reduce our tunneling

Downloaded from http://science.sciencemag.org/ on December 23, 2018

energy to $t/\hbar \approx 2\pi \times 600$ Hz, resulting in a correspondingly lessened experimental time range of $\tau = 1.5\ \hbar/t$ to $4.5\ \hbar/t$.

Figure 3B shows the dependence of $\langle \bar{C} \rangle$ on the strength of added disorder in the AIII-class wire. The measured $\langle \bar{C} \rangle$ values are obtained, as in Fig. 2, through the nonequilibrium bulk dynamics of the atoms after a quench of the tunneling. Because of the restricted range of τ, we include many more disorder configurations (50) to allow for stable measures of $\langle \bar{C} \rangle$. For weak disorder, $\langle \bar{C} \rangle$ rises and reaches a pronounced maximum at $W \approx 2.5$. This is consistent with the expected change in the renormalized m parameter, that is, given the negative sign of the lowest-order correction to m, for weak disorder (*17*, *19*, *34*). $\langle \bar{C} \rangle$ then decays for very strong applied disorder. This observation of an initial increase of $\langle \bar{C} \rangle$ followed by a decrease is indicative of two phase transitions, first from trivial wires to the TAI phase and then to a trivial Anderson insulator at strong disorder, broadened by our finite interrogation time.

Despite the effects of finite-time broadening, we see that our measured $\langle \bar{C} \rangle$ rises to a value greater than 0.5 (the infinite-time $\langle \bar{C} \rangle$ value associated with the critical point) for $W \approx 2.5$, lending further evidence to our observation of the TAI phase. Based on the measurements of $\langle \bar{C} \rangle$ for W = (2.0, 2.5, and 3.0) and their statistical errors, there is only a 0.3% chance for all three measurements to fall below 0.5, the critical value that indicates a change in topology (*30*). Further, the excellent agreement of our experimental $\langle \bar{C} \rangle$ data with a short-time sampled numerical simulation (solid gold line in Fig. 3B), combined with the sharper transitions expected for long-time measurements based on the same simulations (dashed gold line in Fig. 3B for 1000 tunneling times in a 250–unit cell system), provide strong evidence for the observation of disorder-driven topology in an otherwise trivial band structure (*30*).

Unlike condensed-matter systems and photonic simulators, where carrier mobility or lattice parameters may vary from sample to sample, the spectroscopic control of our atomic physics platform has allowed us to engineer many different, precisely tuned realizations of disorder. This level of control will also enable future studies of quantum criticality in disordered topological systems (*9*, *13*). By simple extension to longer evolution times, the interesting physics of logarithmic delocalization at the random-singlet transition may be studied (*14*). Combined with the ability to engineer tunneling phases (*24*) and artificial gauge fields, our technique may be extended to study disordered quantum Hall systems (*13*). And although our present study has been restricted to a regime where interactions are relatively unimportant, the presence of strong interactions in synthetic momentum-space lattices (*35*) will enable future studies of strongly interacting topological fluids.

Note added in proof: After completion and submission of this work, a related work presented complementary evidence for the TAI in photonic waveguide arrays (*36*).

REFERENCES AND NOTES

1. Y. E. Kraus, Y. Lahini, Z. Ringel, M. Verbin, O. Zilberberg, *Phys. Rev. Lett.* **109**, 106402 (2012).
2. D. R. Hofstadter, *Phys. Rev. B* **14**, 2239–2249 (1976).
3. A. Altland, M. R. Zirnbauer, *Phys. Rev. B* **55**, 1142–1161 (1997).
4. S. Ryu, A. P. Schnyder, A. Furusaki, A. W. W. Ludwig, *New J. Phys.* **12**, 065010 (2010).
5. L. Sanchez-Palencia, M. Lewenstein, *Nat. Phys.* **6**, 87–95 (2010).
6. N. Goldman, J. C. Budich, P. Zoller, *Nat. Phys.* **12**, 639–645 (2016).
7. P. W. Anderson, *Phys. Rev.* **109**, 1492–1505 (1958).
8. K. von Klitzing, G. Dorda, M. Pepper, *Phys. Rev. Lett.* **45**, 494–497 (1980).
9. F. Evers, A. D. Mirlin, *Rev. Mod. Phys.* **80**, 1355–1417 (2008).
10. X.-L. Qi, S.-C. Zhang, *Rev. Mod. Phys.* **83**, 1057–1110 (2011).
11. Y. L. Chen *et al.*, *Science* **325**, 178–181 (2009).
12. E. Abrahams, P. W. Anderson, D. C. Licciardello, T. V. Ramakrishnan, *Phys. Rev. Lett.* **42**, 673–676 (1979).
13. H. Aoki, *J. Phys. C Solid State Phys.* **16**, L205–L208 (1983).
14. D. S. Fisher, *Phys. Rev. B* **50**, 3799–3821 (1994).
15. J. Li, R.-L. Chu, J. K. Jain, S.-Q. Shen, *Phys. Rev. Lett.* **102**, 136806 (2009).
16. H. Jiang, L. Wang, Q. Sun, X. C. Xie, *Phys. Rev. B* **80**, 165316 (2009).
17. C. W. Groth, M. Wimmer, A. R. Akhmerov, J. Tworzydło, C. W. J. Beenakker, *Phys. Rev. Lett.* **103**, 196805 (2009).
18. H.-M. Guo, G. Rosenberg, G. Refael, M. Franz, *Phys. Rev. Lett.* **105**, 216601 (2010).
19. A. Altland, D. Bagrets, L. Fritz, A. Kamenev, H. Schmiedt, *Phys. Rev. Lett.* **112**, 206602 (2014).
20. P. Titum, N. H. Lindner, M. C. Rechtsman, G. Refael, *Phys. Rev. Lett.* **114**, 056801 (2015).
21. C. Liu, W. Gao, B. Yang, S. Zhang, *Phys. Rev. Lett.* **119**, 183901 (2017).
22. W. P. Su, J. R. Schrieffer, A. J. Heeger, *Phys. Rev. Lett.* **42**, 1698–1701 (1979).
23. I. Mondragon-Shem, T. L. Hughes, J. Song, E. Prodan, *Phys. Rev. Lett.* **113**, 046802 (2014).
24. E. J. Meier, F. A. An, B. Gadway, *Phys. Rev. A* **93**, 051602 (2016).
25. M. Lohse, C. Schweizer, O. Zilberberg, M. Aidelsburger, I. Bloch, *Nat. Phys.* **12**, 350–354 (2016).
26. S. Nakajima *et al.*, *Nat. Phys.* **12**, 296–300 (2016).
27. C. G. Velasco, B. Paredes, *Phys. Rev. Lett.* **119**, 115301 (2017).
28. J. Billy *et al.*, *Nature* **453**, 891–894 (2008).
29. G. Roati *et al.*, *Nature* **453**, 895–898 (2008).
30. Full details on the experimental and theoretical procedures are available as supplementary materials.
31. E. J. Meier, F. A. An, B. Gadway, *Nat. Commun.* **7**, 13986 (2016).
32. F. Cardano *et al.*, *Nat. Commun.* **8**, 15516 (2017).
33. M. Maffei, A. Dauphin, F. Cardano, M. Lewenstein, P. Massignan, *New J. Phys.* **20**, 013023 (2018).
34. A. Altland, D. Bagrets, A. Kamenev, *Phys. Rev. B* **91**, 085429 (2015).
35. F. A. An, E. J. Meier, J. Ang'ong'a, B. Gadway, *Phys. Rev. Lett.* **120**, 040407 (2018).
36. S. Stützer *et al.*, *Nature* **560**, 461–465 (2018).
37. E. J. Meier *et al.*, Replication data for: Observation of the topological Anderson insulator in disordered atomic wires, Version 1, Harvard Dataverse (2018); https://doi.org/10.7910/DVN/7BMFTD.

ACKNOWLEDGMENTS

We thank N. Goldman, M. Lewenstein, H. Shapourian, and I. Mondragon-Shem for helpful discussions. **Funding:** This material is based upon work supported by the National Science Foundation under grant no. PHY1707731 (E.J.M., F.A.A., and B.G.). A.D., M.M., and P.M. acknowledge Spanish MINECO (Severo Ochoa SEV-2015-0522, FisicaTeAMO FIS2016-79508-P, and SWUQM FIS2017-84114-C2-1-P), the Generalitat de Catalunya (SGR874 and CERCA), the EU (ERC AdG OSYRIS 339106 and H2020-FETProAct QUIC 641122), the Fundació Privada Cellex, a Cellex-ICFO-MPQ fellowship, and the "Ramón y Cajal" program. T.L.H. was supported by the ONR YIP Award N00014-15-1-2383. **Author contributions:** E.J.M. and F.A.A. performed the experiments. E.J.M. analyzed the data. B.G. supervised the experiments and data analysis. A.D., M.M., P.M., and T.L.H. developed the theoretical framework. All authors discussed the results and contributed to the preparation of the manuscript. **Competing interests:** The authors declare no competing financial interests. **Data and materials availability:** All data shown in this work can be found in tables S1 to S3 in the supplementary materials or in an online database (*37*).

SUPPLEMENTARY MATERIALS

www.sciencemag.org/content/362/6417/929/suppl/DC1
Methods
Supplementary Text
Figs. S1 to S7
Tables S1 to S3
References (*38*–*44*)

19 February 2018; accepted 27 September 2018
Published online 11 October 2018
10.1126/science.aat3406

Downloaded from http://science.sciencemag.org/ on December 23, 2018

Science

Observation of the topological Anderson insulator in disordered atomic wires

Eric J. Meier, Fangzhao Alex An, Alexandre Dauphin, Maria Maffei, Pietro Massignan, Taylor L. Hughes and Bryce Gadway

Science **362** (6417), 929-933.
DOI: 10.1126/science.aat3406originally published online October 11, 2018

A messy topological wire

Adding irregularity to a system can lead to a transition from a more orderly to a less orderly phase. Meier *et al.* demonstrated a counterintuitive transition in the opposite direction: Controlled fluctuations in the system's parameters caused it to become topologically nontrivial. The starting point was a one-dimensional lattice of ultracold rubidium atoms in momentum space whose band structure was topologically trivial. The researchers then introduced fluctuations in the tunneling between the lattice sites and monitored the atomic "wires" as the amplitude of the fluctuations increased. The wires first became topologically nontrivial and then went back to trivial for sufficient disorder strengths.

Science, this issue p. 929

ARTICLE TOOLS http://science.sciencemag.org/content/362/6417/929

SUPPLEMENTARY MATERIALS http://science.sciencemag.org/content/suppl/2018/10/10/science.aat3406.DC1

REFERENCES This article cites 44 articles, 1 of which you can access for free
http://science.sciencemag.org/content/362/6417/929#BIBL

PERMISSIONS http://www.sciencemag.org/help/reprints-and-permissions

Use of this article is subject to the Terms of Service

Science (print ISSN 0036-8075; online ISSN 1095-9203) is published by the American Association for the Advancement of Science, 1200 New York Avenue NW, Washington, DC 20005. 2017 © The Authors, some rights reserved; exclusive licensee American Association for the Advancement of Science. No claim to original U.S. Government Works. The title *Science* is a registered trademark of AAAS.

Downloaded from http://science.sciencemag.org/ on December 23, 2018